SUPPLEMENTAL INFORMATION

Supplemental Data

Figure S1 Related to Figure 1

Patchy feedback projections from area AL to mouse V1

(A) Tangential section through posterior third of left cortex showing axonal connections from area AL to V1, LM, POR, LI, RL, A, S1, S2, AM and PM labeled by injecting AAV2/1.pSyn1.EGFP.WPRE.bGH into area AL. The injection site is centered in AL, which is identified by its location anteromedially of the strongly M2-expressing area LM (B) (Wang et al., 2011). (C) Overlay of (A) and (B). Boxed area in A-C is shown at higher magnification in Figure 1D-F. Abbreviations same as in Figure 2.

Figure S2 Related to Figure 1

Optical density maps of patchy projections to L1 of mouse V1

Optical density maps of AAV2/1.pSyn1.EGFP.WPRE.bGH labeled inputs from the dLGN (A) and area AL (B) to L1 of mouse V1. Crosses indicate peaks of patchy projections. Scale bars 100 µm. (C, D) Boxplots of relative projection densities expressed as ratios between inputs to patches and interpatches. Although intracortical FB inputs and dLGN projections are clustered, the contrast between patches and interpatches is significantly greater for inputs from AL, RL (C) and dLGN (D) than for inputs from LM (C, D).

Figure S3 Related to Figure 2

Patchy expression of M2 in L1 of rat visual cortex

M2 expression in tangential section through L1 of rat visual cortex. The patchiness is more pronounced in the posterior than the anterior part of V1, indicating a downward tilt in the plane of section away from the pial surface to the bottom of layer 1. The patchy M2 expression pattern extends across V1 and includes areas LM, LI, P and POR of lateral extrastriate visual cortex.

Notice that similar to mouse, M2 expression in AL and cortex anterior and medial to V1 is weak and uniform. Lateral (L), anterior (A). Scale bar: 1 mm

Figure S4 Related Figure 2

Patchy expression of M2 in L1 of monkey V1

(A) Patchy M2 expression in tangential section (160 µm below the pial surface) through L1. Arrows indicate matching locations in A and B. (B) Complementary patterns of M2+ (red) and cytochrome oxidase-expressing patches (green). Scale (1mm).

Figure S5 Related to Figure 5

Recording sites in L2/3 aligned with M2+ and M2- zones in L1 of mouse V1.

Optical density map of M2 expression in L1 of V1. M2 peaks (+). Black lines denote Voronoi polygons. Recoding sites marked with DiI (purple) of L2/3 neurons aligned with M2+ (1) and M2- (2) zones in L1 whose responses are shown in Figure S6. Scale: 100 µm.

Figure S6 Related to Figure 8

Distinct combinations of spatiotemporal properties of L2/3 neurons aligned with M2+ and M2- zones in mouse V1

(A-G) Mean tuning curves (± SEM) to 10 repetitions of different stimulus variables recorded in M2+ (red) and M2- (black) zones at the sites 1 and 2 shown in Figure S5. Solid lines indicate best fitting functions (Gao et al., 2010). Dashed lines represent average spontaneous activity. DI (discrimination index). Peak (maximal response). Slope (derived from linear fit). C50 (contrast at which response magnitude is 50% of peak). HWHM (half width at half maximal response). Orientation (A), direction (B), speed of motion (C), motion coherence (D), contrast (E), spatial frequency (F), temporal frequency (G). Notice that the red neuron is optimally tuned for orientation, low speed, lacks motion coherence selectivity, shows moderate contrast sensitivity, is selective for high spatial frequency and low temporal frequency. In contrast, the black neuron

lacks orientation selectivity, is sharply tuned for direction, prefers high speeds, is tuned for motion coherence, shows moderate contrast sensitivity, prefers low spatial frequency and high temporal frequency.

Figure S7 Related to Figure 8

Tuning strengths in L2/3 neurons aligned with M2+ and M2- zones in L1 of mouse V1

Discrimination index (DI, which measures tuning strength for different visual stimuli of L2/3 neurons in M2+ (red) and M2- (black) zones of V1. (A) Orientation selectivity (OS). (B) Direction selectivity (DS). (C) Speed selectivity (SS). (D) Motion Contrast selectivity (MCS). Contrast selectivity (CS). Spatial frequency selectivity (SF). G, Temporal frequency selectivity (TF). H, Median peak speed in M2+ and M2- zones. Significance assessed with Mann-Whitney *U* test.

Supplemental Experimental Procedures

All experimental procedures were approved by the Institutional Animal Care and Use Committee at Washington University and conformed to the National Institutes of Health guidelines.

Animals. Experiments were performed in 5-8 week-old male and female wild type C57BL/6J, and C57BL/6-M2$^{-/-}$ mutant (Gomeza et al., 1999; gift from Jürgen Wess, National Institute of Diabetes, Digestive and Kidney Diseases) mice and 4-month old male Long-Evans rats. The visual cortex of a 9-year old male rhesus monkey (*Macaca mulatta*), involved in a terminal study unrelated to the present investigation was obtained (gift from Lawrence Tychsen, Washington University School of Medicine). The monkey was euthanized with an overdose of pentobarbital (150 mg/kg, IV) and perfused with heparinized 0.1 M phosphate buffer (pH 7.4, PB) followed by 4% paraformaldehyde in PB.

Tracing of connections. Connections were labeled by anterograde and retrograde tracing of neuronal pathways. Mice were anesthetized with ketamine/xylazine (86 mg·kg^{-1}/13 mg·kg^{-1}, IP)

and secured in a headholder. Analgesia was achieved by Buprenorphine (0.05 mg·kg-1, SC). Pressure injections were made with glass pipettes (tip diameter 10-20 µm) connected to either a Nanoject II (Drummond) or a Picospritzer (Parker-Hannafin). Axonal inputs to the left V1 were traced by injecting the dLGN (from bregma posterior/lateral/depth in mm: -2.35/ 2.25/2.5), LM (from transverse sinus anterior/lateral/depth in mm:1.4/4.1/0.35), AL (2.3/3.6/0.35), or RL (2.8/3.3/0.35) with AAV2/1.pSyn1.EGFP.WPRE.bGH (10 x 4.6 nl; Vector Core, University of Pennsylvania). Callosal connections were labeled by retrograde tracing with bisbenzimide (30 injections 20 nl each, 5% in H_2O, Sigma) from the right occipital cortex. To allow for axonal transport of tracer, postsurgical survival times were 4 days for bisbenzimide and 21 days for the virus.

Immunostaining. Mice and rats were overdosed with ketamine/xylazine, perfused through the heart with heparinized PB followed by either 1% or 4% paraformaldehyde in PB. The monkey occipital lobes were flatmounted and postfixed in 4% paraformaldehyde and equilibrated in 30% sucrose. Rodent brains were postfixed with 4% paraformaldehyde, sunk in 30% sucrose, and cut on a freezing microtome at 40µm in the coronal plane. In rodent brains fixed with 1% paraformaldehyde, the left cortical hemisphere was removed, flatmounted (Wang et al., 2012), postfixed in 4% paraformaldehyde and cryoprotected in 30% sucrose. Flatmounted monkey and rodent cortices were cut on a freezing microtome at 40 µm in the tangential plane. To reveal bisbenzimide labeled landmarks in mice, sections were wet mounted on glass slides in PB and imaged under UV illumination under a microscope equipped with a CCD camera. The sections were then removed from the slides, treated with normal goat serum (10% NGS / 0.01% Triton X-100) in PB and incubated with an antibody against the M2 muscarinic acetylcholine receptor (1:500 in PB; MAB367; Millipore). Next, the sections were treated with Alexa Fluor 647-labeled secondary antibody (1:500 in 10% NGS; A21247; Invitrogen). The same M2-staining protocol was used for monkey sections, which were subsequently histochemically stained for CO activity

(Tootell et al., 1988). Selected sections were counterstained for Nissl substance with NeuroTrace 435/455 (Invitrogen). Sections were mounted onto glass slides, coverslipped in PB or DPX and imaged with a CCD camera (CoolSnap EZ, Roper Scientific) using appropriate wavelengths for visualizing green, red and IR fluorescence, including bright field illumination.

Analysis of M2 expression. For quantitative analysis of M2 expression in horizontal sections, we used customized software (Matlab, MathWorks) to determine the optical density of immunostaining. Immunofluorescence was converted to gray-tone images which were Gaussian filtered at 5 µm. We then found the region in which staining density was maximal, subtracted the background, and generated contour maps of the difference in optical densities, by plotting iso-density lines at 10% intervals. Because the cutting plane was not always perfectly parallel to the plane of a layer and section thickness was variable, the absolute optical density often differed across a section. We therefore, thresholded the optical density in regions of similar overall staining intensity at 70% of the local peak, determined the centroid (ImageJ, NIH) of each patch and displayed the M2 pattern as a distribution of centroid locations across V1. These maps were then used to derive centroid density profiles, which plots the probability within a 200 µm radius around centroids, in a 1.2 x 1. 2 mm-wide region for finding another centroid (Rodieck et al., 1991). We computed the probability by measuring for each reference centroid the distances to all the other centroids and plotted the histogram as a function of centroid density within 20 µm-wide annuli of increasing radius. The distance at which the mean centroid density plateaued and reached the value of a random distribution at the same centroid density was the radius of the region of exclusion around each centroid.

The centroids were further used as seed points to generate a Voronoi diagram of V1 using customized Python 2.7.2 software. Voronoi polygons represent domains of graded M2 expression, which is maximal at the centroid and near minimal along the perimeter. To

determine the size of domains across V1, we overlaid the tessellated map of M2 expression with the retinotopic grid of Marshel et al (2011) by aligning the V1 border to the outline of intense immunostaining in L4. For each 10 x 10 deg (azimuth x elevation) tile we computed the mean distance between centroids (i.e. axial lengths of domains) along azimuth and elevation. The number of domains within a 10 x 10 deg tile was $N = \Sigma k$, where k represents the fraction of every polygon inside a tile (k = 1 if the entire polygon is inside a tile, k = 0 if the polygon is outside, $0 < k < 1$ represents the fraction of the polygon inside a tile). The spatial mosaic of M2 patches was determined from the relationship between centroids, using an approach similar to that employed for the analysis of the patchy pattern of neuronal activity in superficial layers of cat and monkey V1 (Muir et al., 2011). For each centroid, all its neighbors were identified by Gabriel graphing (Gabriel and Sokal, 1969). Next, we determined the distribution of the interior angles between neighbors (interneighbor angles) and used bootstrap analysis (Efron, 1979) to estimate the confidence intervals at 95% confidence level. Then, we compared the interneighbor angles, using the 2-sided Kolmogorov-Smirnov (K-S) test against random distributions drawn from a Poisson process, as well as against square and hexagonal lattices with uniform origin, orientation and spacing equal to the average distance between centroids (Neyman and Scott, 1958). Finally, we extended the analysis by generating lattices of different orientation, each of them jittered by amounts varying from 0 (perfect square of hexagonal lattice) to 1 (Poisson process). The interneighbor angles were recorded for each condition and a 2-sided K-S test was performed to evaluate the similarity with the data.

Visual stimulation. Drifting sinusoidal gratings (peak luminance of white stripes 75 cd/m^2, dark stripes 2 cd/m^2) were used for examining selective tuning for orientation (OS; at maximum contrast, fixed at 0.03 c/deg spatial frequency at 12 different orientations 30 deg apart), contrast (CS; fixed at optimal orientation and drift speed, contrasts varied from 1% to 100%), spatial frequency (SF; optimal orientation, maximum contrast, spatial frequency varied from 0.01 to 0.8

c/deg) and temporal frequency (TF; optimal orientation, maximum contrast, spatial frequency 0.03 c/deg, drifting at 0.5-16 Hz). Drifting patterns of random dots (peak luminance of white dots 75 cd/m^2, 3 deg in diameter, displayed at a density of 0.5 dots/deg^2/s) on a dark background (2 cd/m^2) were used to examine selectivity for direction of motion (DS), speed (SS) and motion coherence (MCS). For measuring DS and SS tuning, random-dot stimuli were fully coherent with dots wrapping around after reaching the edge of the aperture. DS was tested at 8 directions of motion in increments of 45 deg at fixed speed of 10 deg/s. SS was measured by varying speed from 1 to 128 deg/s at the optimal direction of motion. For measuring MCS a variable fraction of dots moved coherently (dwell time of 50 ms), while the rest of the dots were randomly replotted within the aperture. The stimulus resembled dynamic noise when equal proportions of dots moved in different directions. The behaviorally determined MCS threshold in pigmented rats is 10-20% coherence, which is slightly more sensitive than that of mouse V1 neurons in (Hupfeld and Hoffmann, 2006; Gao et al, 2010). The screen between trials was uniformly gray at 35 cd/m^2. All stimuli were generated by a Quadro FX 1400 accelerator board supported by Open GL 2.1 and were displayed on a 22 inch flat screen LCD monitor with 120 Hz refresh rate and 2 ms video response time (View Sonic GeForce 3D vision). The display was placed at a fixed 22.5 cm viewing distance, subtending 67 x 92 deg, and was mounted to a system of articulated arms that allowed universal positioning on a virtual sphere centered on the right eye.

Single unit recordings. For single unit recordings mice were anesthetized with urethane (20% in PBS, 0.2ml/20 g body weight, IP), injected with atropine (1.7 mg/kg, SC) to reduce tracheal secretions and methylprednisolone sodium succinate (2%, 0.01ml, IM) to prevent brain swelling. Mice were positioned in a headholder with the incisor bar 2.5 mm below the interaural line. Body temperature was maintained at 37ºC with a feedback controlled heating pad. The eyes were protected with a thin layer of ophthalmic ointment (Neomycin and Polymyxin B Sulfates and Bacitracin Zinc Ophthalmic Ointment, Akorn) which for recording of visual responses was

replaced by a thin layer of low viscosity silicone oil (30,000 cSt, Sigma) to prevent drying of the cornea. Using stereotaxic coordinates, the approximate border of the left V1 was outlined by 3 points (anterior to the transverse sinus/lateral to midline in mm): 1/3.5; 1.5/2.0, 3/2.5. Within this border small (0.3 mm in diameter) craniotomies were made at different topographic locations of the visual field (Wang and Burkhalter, 2007). For recording we used lacquer-coated tungsten microelectrodes, manufactured from 125-µm wire (Midwest Tungsten Service), with tip diameters of 2-5 µm and 1-2 MΩ resistance. Recording sites were marked by painting electrodes with DiI (1,1' - Dioctadecyl - 3,3,3',3' - tetramethylindocarbocyanine iodide; 5% in absolute ethanol; Invitrogen) (DiCarlo et al., 1996). Recording depth was measured as the distance from the pial surface and was monitored with a micromanipulator (Sutter Instruments). The exposed surface of the brain was protected with a thin layer of petroleum jelly. Single units were isolated using a digital neural spike discriminator (FHC). Spike responses were acquired with TEMPO software (Tempo, Reflective Computing). Neural signals were amplified and bandpass filtered at 300-5000 Hz, using the Axoprobe-2A amplifier (Molecular Devices). Spikes along with event markers were stored at 1 ms resolution in a computer.

Mapping of receptive fields. Searching for a RF was done by moving a light bar on the black screen and listening to the audiomonitor output of spike discharge. The size of a RF was mapped quantitatively by presenting a circular patch (5 deg in diameter) of a drifting sinusoidal grating (0.03 c/deg) at various locations on the monitor screen. The response of a neuron was computed as the mean firing rate over the 2 s stimulus duration. RF size was determined from spatial response plots in which points representing similar mean response strengths were connected by contour lines. The contour corresponding to 2 standard deviations (SDs) of the fitted Gaussian was used to determine the dimensions of a RF. This was done by transforming elliptical into circular fields and computing the diameter. RF location was determined on a virtual sphere centered on the pupil of the right eye. The vertical meridian was the intersection

between the sphere and the parasagittal plane through the tip of the nose. The horizontal meridian was the intersection between the sphere and the horizontal plane through the center of the eye. Within this reference frame azimuth and elevation of the center of RFs were measured with a digital protractor (iGaging).The overlap between neighboring RFs was computed as the absolute value of the difference of the distance between RF centers and the sum of the RF radii. RF overlap was plotted against the distance between recording sites and the distribution was fit by linear regression. The distance at which this curve intercepted the zero-line was taken as the distance between non-overlapping RFs.

Analysis of single unit data

The analysis of neural responses was similar to the methods used in a previous study (Gao et al., 2010). Responses for each trial were computed as mean firing rate over 2 s stimulus duration. ANOVA was used to assess significant ($p < 0.05$) tuning. Tuning curves were fit with functions that best described the data with a small number of parameters. OS tuning curves were fit with the sum of two modified von Mises functions, which were used to compute peak responses. SF and TF tuning curves were fit with log Gaussian functions from which we extracted response peak and tuning width (i.e. half width at half maximal height (HWHM)). CS tuning was fit with a hyperbolic ratio function. DS tuning was fit with a Gaussian. SS tuning was fit with a gamma function. SS tuning width was computed as half width at half maximal response. MCS was fit with a linear function.

From each OS, SF, TF, CS, DS SS and MCS tuning curve we extracted a discrimination index (DI) with measures the tuning strength. The DI was $DI= (R_{max}-R_{min})/[(R_{max}-R_{min}) + 2\sqrt{SSE/(N-M)}]$ were R_{max} is the mean response to the most effective and R_{min} to the least effective stimulus. SSE denotes the sum squared error around the mean responses. N is the number of trials and M is the number of values tested. A DI of ≥ 0.425 which corresponds to a ~ 2:1 modulation was

taken as significant tuning. The non-paramedic Mann-Whitney *U* test was used to compare the properties between groups. The variability of mean responses is indicated by SEM.

Supplemental References

DiCarlo, J.J., Lane, J.W., Hsiao, S.S., and Johnson, K.O. (1996). Marking microelectrode penetrations with fluorescent dyes. J Neurosci Methods *64*, 75-81.

Efron, B. (1979). Bootstrap methods: another look at the jackknife. The 1977 Rietz lecture. Ann Stat *7*, 1-26.

Gomeza, J., Shannon, H., Kosteins, E., Felder, C., Zhang, L., Brodkin, J., Grinberg, A., Sheng, H., and Wess, J. (1999). Pronounced pharmacologic deficits in M2 muscarinic acetylcholine knockout mice. Proc Natl Acad Sci USA *96*, 1692-1697.

Hupfeld, D., Hoffmann, K.-P. (2006). Motion perception in rats (*Rattus norvegicus* sp.): Deficits in albino Wistar rats compared to pigmented Long-Evans rats. Behav Brain Res *170*, 29-33.

Wang, Q., Gao, E., and Burkhalter, A. (2011). Gateway of ventral and dorsal streams in mouse visual cortex. J Neurosci *31*,1905-1918.

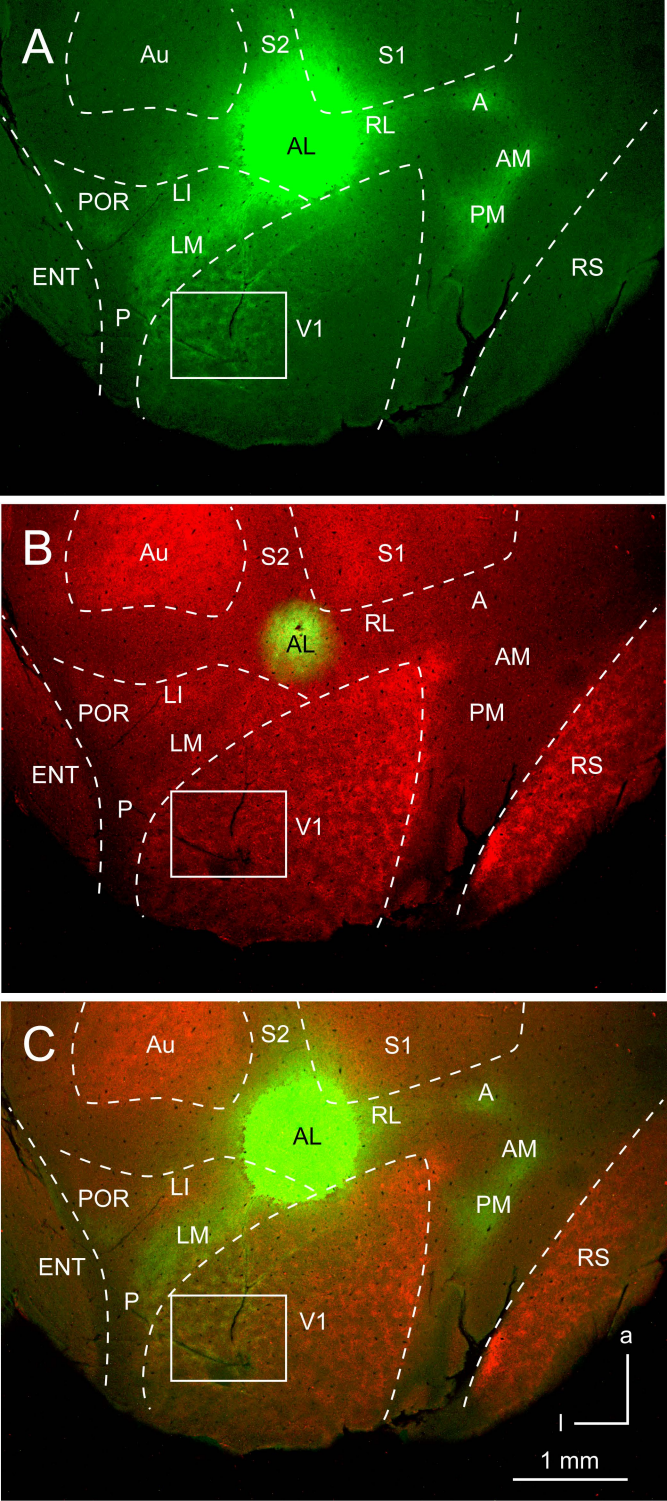
A
Au
S2
S1
A
RL
AL
AM
POR
LI
PM
LM
ENT
RS
P
V1
B
Au
S2
S1
A
RL
AL
AM
POR
LI
PM
LM
ENT
RS
P
V1
C
Au
S2
S1
A
RL
AL
AM
POR
LI
PM
LM
ENT
RS
P
V1
a
l
1 mm

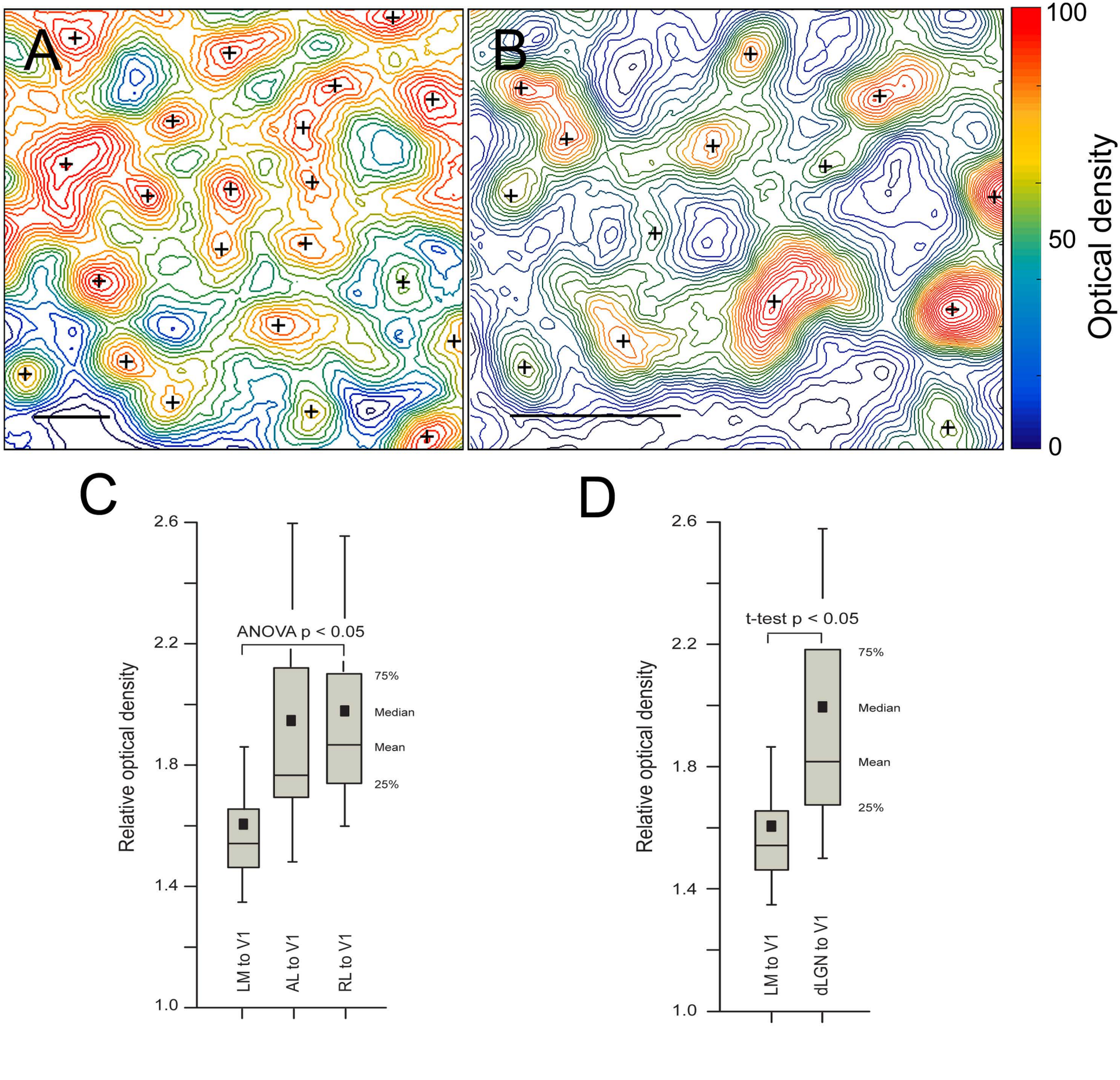
A
B
100
50
0
Optical density
C
D
2.6
2.2
1.8
1.4
1.0
Relative optical density
ANOVA p < 0.05
t-test p < 0.05
75%
Median
Mean
25%
LM to V1
AL to V1
RL to V1
dLGN to V1

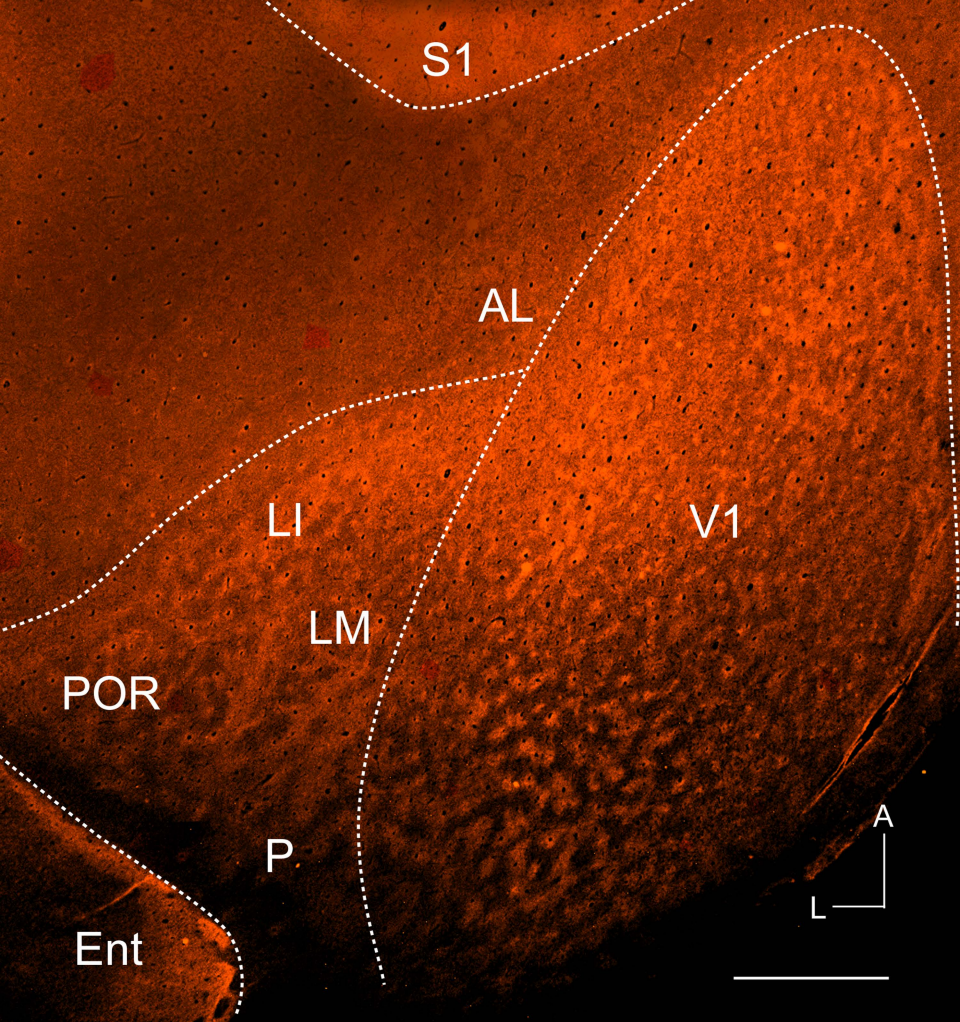
S1
AL
LI
V1
LM
POR
P
Ent
A
L

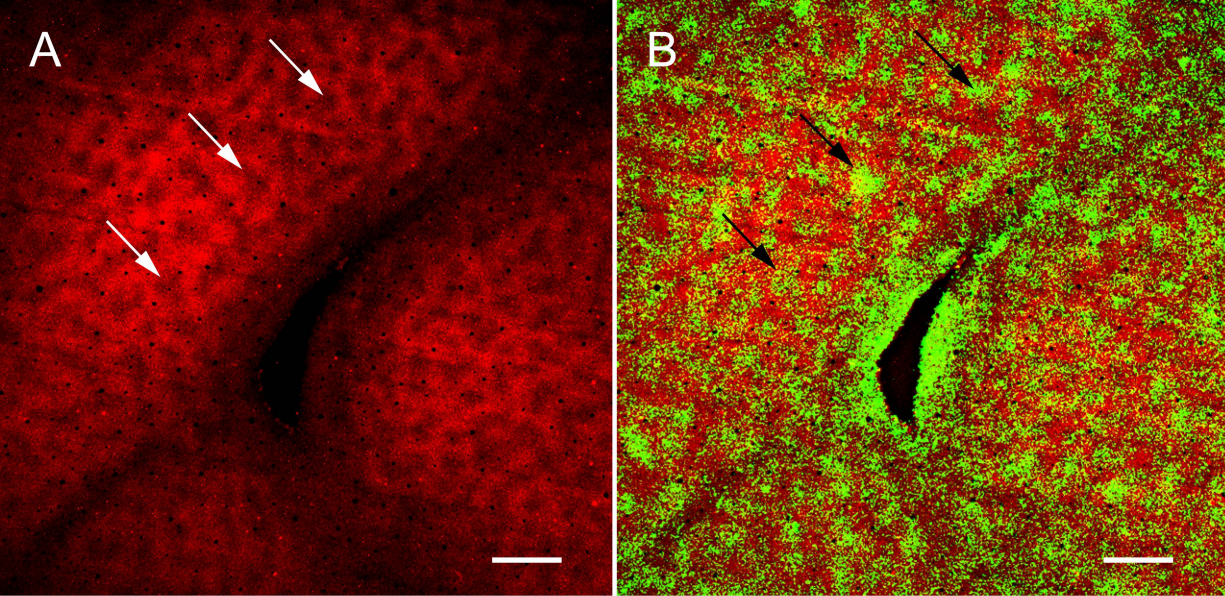
A
B

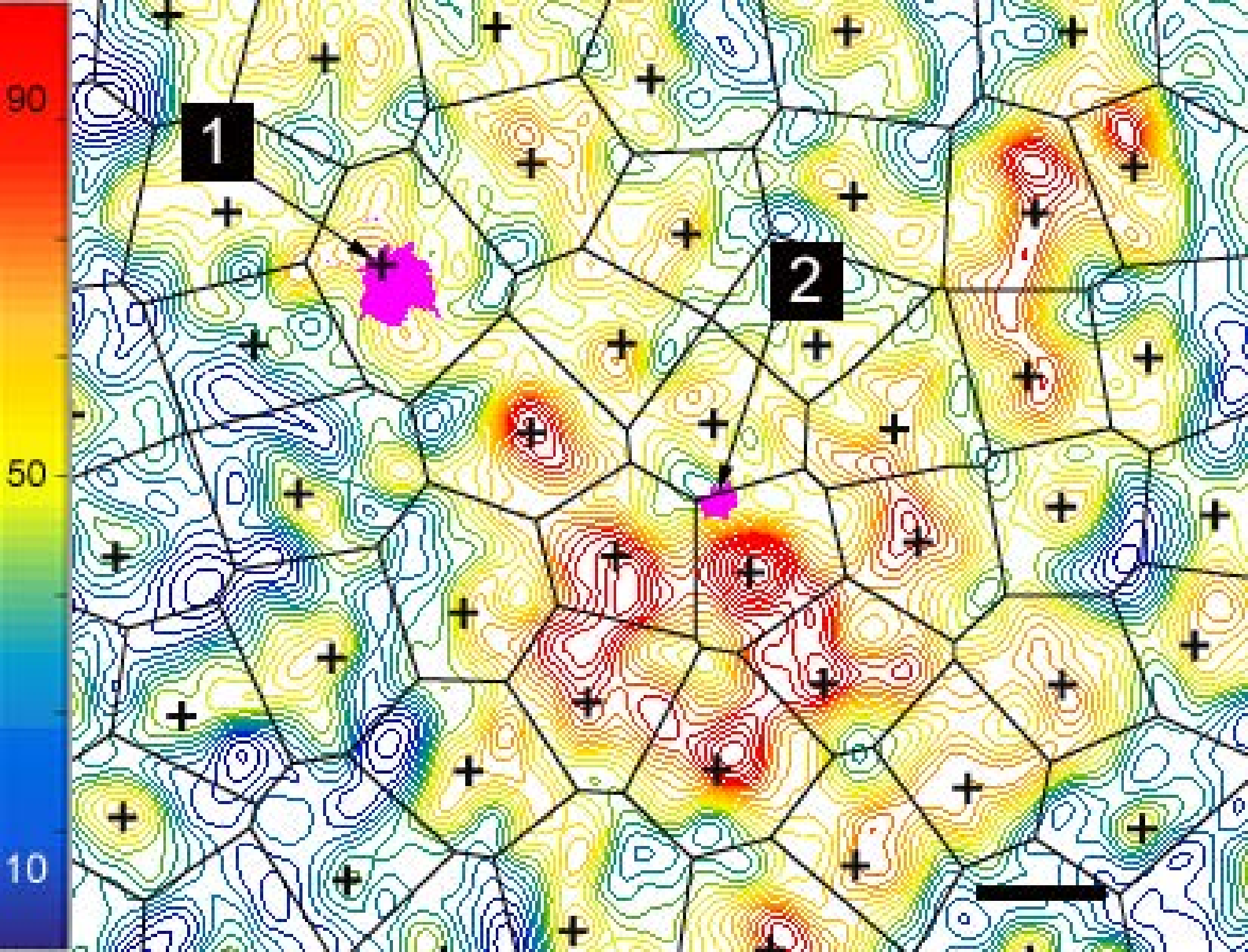
90
50
10
1
2

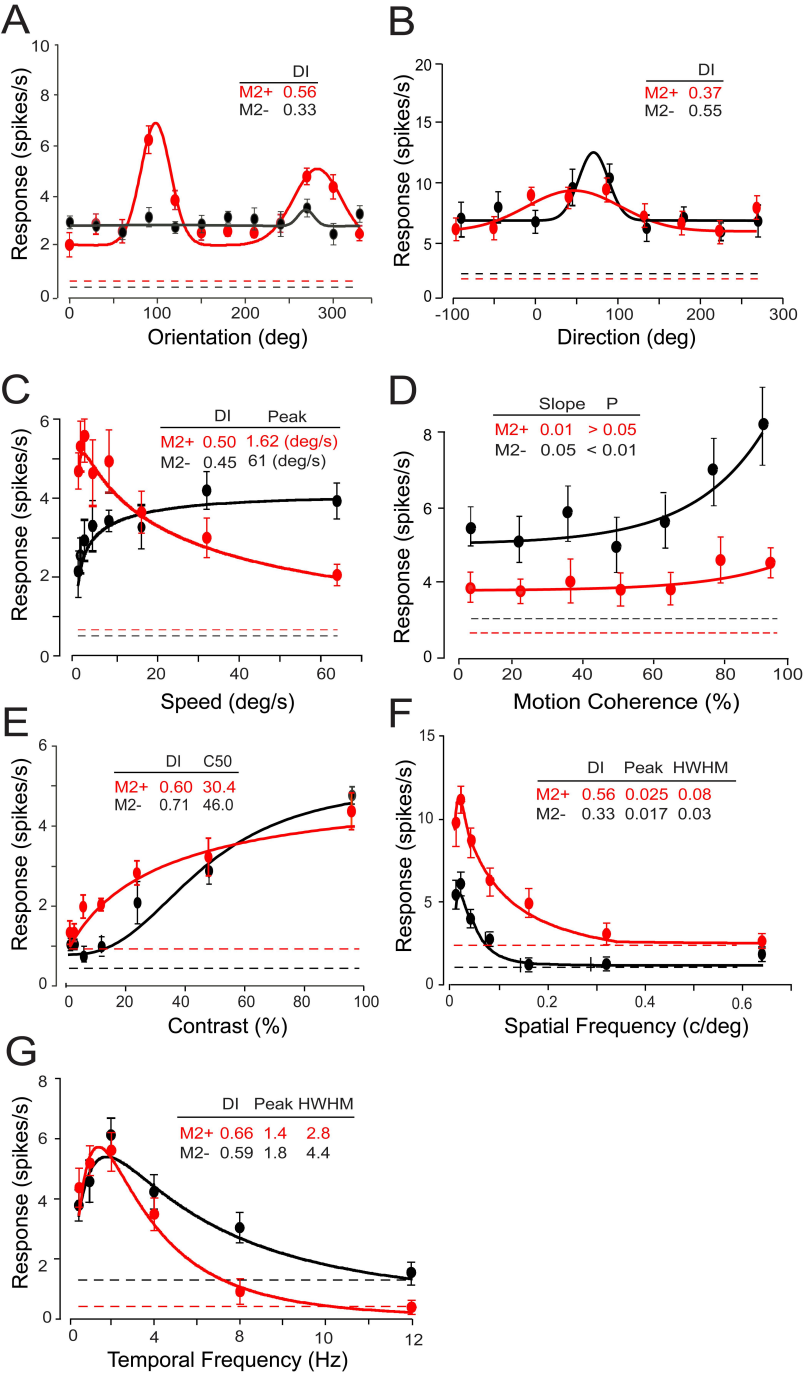
A
Response (spikes/s)
Orientation (deg)
DI
M2+ 0.56
M2- 0.33
B
Response (spikes/s)
Direction (deg)
DI
M2+ 0.37
M2- 0.55
C
Response (spikes/s)
Speed (deg/s)
DI Peak
M2+ 0.50 1.62 (deg/s)
M2- 0.45 61 (deg/s)
D
Response (spikes/s)
Motion Coherence (%)
Slope P
M2+ 0.01 > 0.05
M2- 0.05 < 0.01
E
Response (spikes/s)
Contrast (%)
DI C50
M2+ 0.60 30.4
M2- 0.71 46.0
F
Response (spikes/s)
Spatial Frequency (c/deg)
DI Peak HWHM
M2+ 0.56 0.025 0.08
M2- 0.33 0.017 0.03
G
Response (spikes/s)
Temporal Frequency (Hz)
DI Peak HWHM
M2+ 0.66 1.4 2.8
M2- 0.59 1.8 4.4

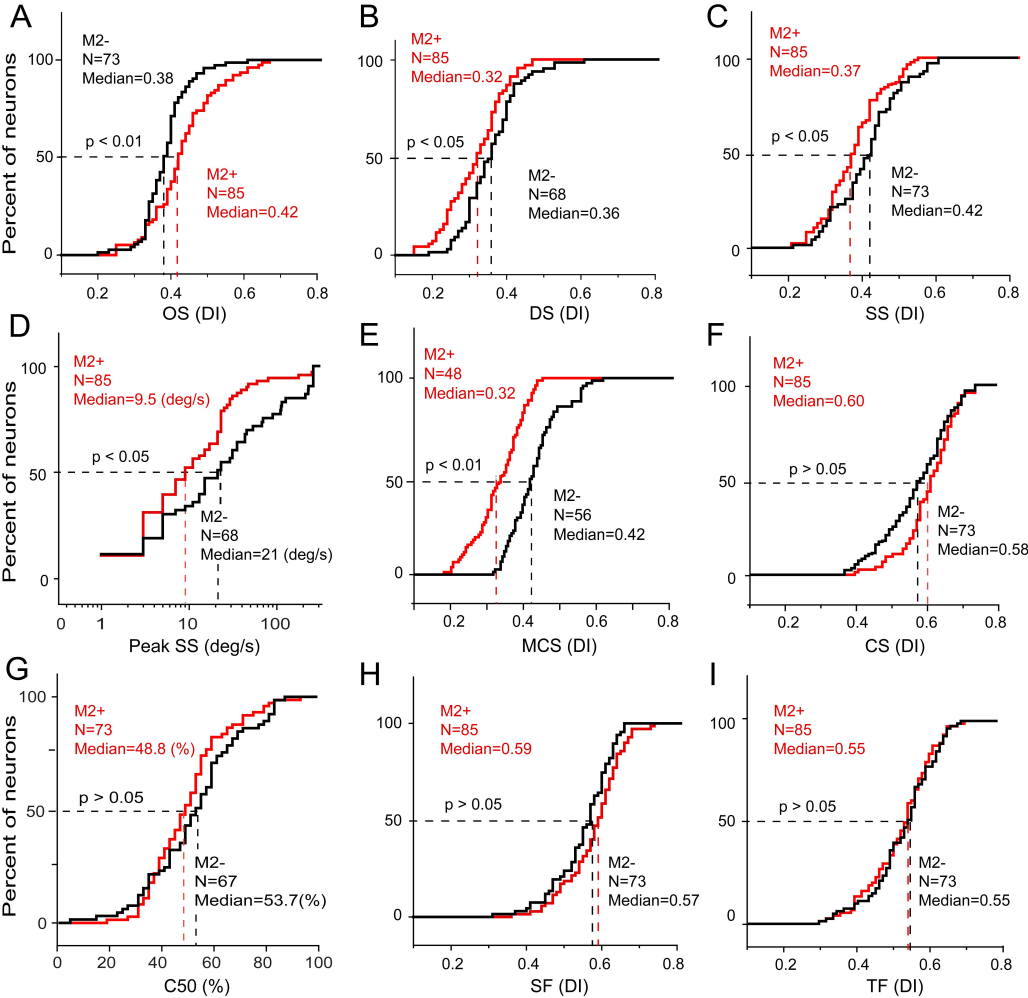
A
M2-
N=73
Median=0.38
p < 0.01
M2+
N=85
Median=0.42
Percent of neurons
OS (DI)
B
M2+
N=85
Median=0.32
p < 0.05
M2-
N=68
Median=0.36
DS (DI)
C
M2+
N=85
Median=0.37
p < 0.05
M2-
N=73
Median=0.42
SS (DI)
D
M2+
N=85
Median=9.5 (deg/s)
p < 0.05
M2-
N=68
Median=21 (deg/s)
Percent of neurons
Peak SS (deg/s)
E
M2+
N=48
Median=0.32
p < 0.01
M2-
N=56
Median=0.42
MCS (DI)
F
M2+
N=85
Median=0.60
p > 0.05
M2-
N=73
Median=0.58
CS (DI)
G
M2+
N=73
Median=48.8 (%)
p > 0.05
M2-
N=67
Median=53.7(%)
Percent of neurons
C50 (%)
H
M2+
N=85
Median=0.59
p > 0.05
M2-
N=73
Median=0.57
SF (DI)
I
M2+
N=85
Median=0.55
p > 0.05
M2-
N=73
Median=0.55
TF (DI)